

Alma Mater Studiorum Università di Bologna  
Archivio istituzionale della ricerca

Improved centrifugal and hyperfine analysis of ND<sub>2</sub>H and NH<sub>2</sub>D and its application to the spectral line survey of L1544

This is the final peer-reviewed author's accepted manuscript (postprint) of the following publication:

*Published Version:*

Improved centrifugal and hyperfine analysis of ND<sub>2</sub>H and NH<sub>2</sub>D and its application to the spectral line survey of L1544 / Melosso M.; Bizzocchi L.; Dore L.; Kisiel Z.; Jiang N.; Spezzano S.; Caselli P.; Gauss J.; Puzzarini C.. - In: JOURNAL OF MOLECULAR SPECTROSCOPY. - ISSN 0022-2852. - STAMPA. - 377:(2021), pp. 111431.111431-1-111431.111431-8. [10.1016/j.jms.2021.111431]

*Availability:*

This version is available at: <https://hdl.handle.net/11585/867650> since: 2022-02-24

*Published:*

DOI: <http://doi.org/10.1016/j.jms.2021.111431>

*Terms of use:*

Some rights reserved. The terms and conditions for the reuse of this version of the manuscript are specified in the publishing policy. For all terms of use and more information see the publisher's website.

This item was downloaded from IRIS Università di Bologna (<https://cris.unibo.it/>).  
When citing, please refer to the published version.

(Article begins on next page)

This is the final peer-reviewed accepted manuscript of:

**M. Melosso, L. Bizzocchi, L. Dore, Z. Kisiel, N. Jiang, S. Spezzano, P. Caselli, J. Gauss, C. Puzzarini. Improved centrifugal and hyperfine analysis of ND<sub>2</sub>H and NH<sub>2</sub>D and its application to the spectral line survey of L1544. J. Mol. Spectrosc. 377 (2021) 111431**

The final published version is available online at:

<https://doi.org/10.1016/j.jms.2021.111431>

Terms of use:

Some rights reserved. The terms and conditions for the reuse of this version of the manuscript are specified in the publishing policy. For all terms of use and more information see the publisher's website.

*This item was downloaded from IRIS Università di Bologna (<https://cris.unibo.it/>)*

***When citing, please refer to the published version.***

# Improved centrifugal and hyperfine analysis of ND<sub>2</sub>H and NH<sub>2</sub>D and its application to the spectral line survey of L1544

Mattia Melosso<sup>a,\*</sup>, Luca Bizzocchi<sup>b</sup>, Luca Dore<sup>a</sup>, Zbigniew Kisiel<sup>c</sup>, Ningjing Jiang<sup>a</sup>, Silvia Spezzano<sup>b</sup>, Paola Caselli<sup>b</sup>, Jürgen Gauss<sup>d</sup>, Cristina Puzzarini<sup>a,\*</sup>

<sup>a</sup>*Dipartimento di Chimica “Giacomo Ciamician”, Università di Bologna, Via F. Selmi 2, 40126 Bologna, Italy*

<sup>b</sup>*Center for Astrochemical Studies, Max Planck Institut für extraterrestrische Physik, Gießenbachstraße 1, 85748 Garching bei München, Germany*

<sup>c</sup>*Institute of Physics, Polish Academy of Sciences, Al. Lotników 32/46, 02-668 Warszawa, Poland*

<sup>d</sup>*Department Chemie, Johannes Gutenberg-Universität Mainz, Duesbergweg 10-14, 55128 Mainz, Germany*

---

## Abstract

Quantifying molecular abundances of astrochemical species is a key step towards the understanding of the chemistry occurring in the interstellar medium. This process requires a profound knowledge of the molecular energy levels, including their structure resulting from weak interactions between nuclear spins and the molecular rotation. With the aim of increasing the quality of spectral line catalogs for the singly- and doubly-deuterated ammonia (NH<sub>2</sub>D and ND<sub>2</sub>H), we have revised their rotational spectra by observing many hyperfine-resolved lines and more accurate high-frequency transitions. The measurements have been performed in the submillimeter-wave region (265–1565 GHz) using a frequency modulation submillimeter spectrometer and in the far-infrared domain (45–220 cm<sup>-1</sup>) with a synchrotron-based Fourier-transform interferometer. The analysis of the new data, with the interpretation of the hyperfine structure supported by state-of-the-art quantum-chemical calculations, led to an overall improvement of all spectroscopic parameters. Moreover, the effect of the inclusion of deuterium splittings in the analysis of astrophysical NH<sub>2</sub>D emissions at millimeter wavelengths has been tested using recent observations of the starless core L1544, an ideal astrophysical laboratory for the study of deuterated species. Our results show that accounting for hyperfine interactions leads to a small but significant change in the physical parameters used to model NH<sub>2</sub>D line emissions.

*Keywords:* Ammonia, Hyperfine structure, Rotational spectroscopy, Interstellar medium, Deuterium fractionation, Starless core

---

## 1. Introduction

The increasing sensitivity and spectral resolution of modern radio-telescopes are stimulating a large number of laboratory studies that aim at supporting astronomical observations of molecules in the Interstellar Medium (ISM). On the one hand, these studies mostly exploit rotational spectroscopy techniques to characterize small- to medium-sized species, the reason being that rotational signatures can undoubtedly prove (and quantify) the presence

of a molecule in the ISM [1]. On the other hand, laboratory efforts on a particular molecular system can be motivated by several aspects. Among them, the search for pre-biotic species and molecules that are more generally related to the origin of life is still one of the hottest topics in astrochemistry [2, 3, 4], although any attempt to detect amino acids in the gas-phase has so far remained unsuccessful [5, 6]. However, being evident that the ISM exhibits a complex chemistry, the characterization of new Complex Organic Molecules (COMs, i.e. species containing at least six atoms and composed of carbon, hydrogen, oxygen and/or nitrogen) is the main theme of joint laboratory-observational studies [7, 8, 9, 10]. Moreover, the new detections of

---

\*Corresponding authors

*Email addresses:* [mattia.melosso2@unibo.it](mailto:mattia.melosso2@unibo.it) (Mattia Melosso), [cristina.puzzarini@unibo.it](mailto:cristina.puzzarini@unibo.it) (Cristina Puzzarini)

ions [11], radicals [12], carbon-chains [13, 14], and rings [15] –including aromatic ones [16]– open new perspectives for an even richer molecular complexity.

All these aspects contribute to our understanding of the interstellar chemistry and are useful to probe excitation mechanisms and kinematics, as well as to trace the evolutionary stage of astronomical objects [17, 18] and their chemical differentiation [19, 20, 21]. However, the evaluation of molecular abundances, which are in turn the building-blocks of astrochemical models, is a crucial point that requires a deep knowledge of the molecule under investigation: this can include information about vibrational excited states [22, 23], a correct computation of partition function values [24], or the effect of nuclear electric and magnetic interactions giving raise to the so-called hyperfine structures (HFS).

Recently, the importance of such effects in the analysis of singly-deuterated ammonia (NH<sub>2</sub>D) line emission towards the starless core H-MM1 has been pointed out [25, 26] and, subsequently, addressed in our laboratory in Bologna [27]. In the context of a broader investigation of the rotational spectra of ammonia isotopologues, we have extended the centrifugal analysis of NH<sub>2</sub>D and ND<sub>2</sub>H at higher frequencies and measured additional hyperfine-resolved transitions, especially those of astronomical interest. The new measurements have been combined with literature data to obtain the best set of spectroscopic constants for both singly- and doubly-deuterated ammonia, in order to generate accurate line catalogs. Then, the effect of including deuterium hyperfine interactions on the analysis of astrophysical NH<sub>2</sub>D emissions at millimeter wavelengths has been tested using recent observations of the low-mass star-forming core L1544.

The paper is organized as follows. First, the spectral features of the rotation-inversion spectrum of ND<sub>2</sub>H compared to that of NH<sub>2</sub>D (Section 2) are presented. Then, the submillimeter spectrometer and the synchrotron-based Fourier transform interferometer used for the measurements are described (Section 3). In Section 4, the results of our spectral analysis are given and applied to NH<sub>2</sub>D line emissions towards the starless core L1544. Finally, our findings are summarized in Section 5.

## 2. Theory

The main features of the rotational spectrum of NH<sub>2</sub>D have been exhaustively described in Melosso *et al.* ([27], hereafter **Paper I**). The spectroscopic behavior of ND<sub>2</sub>H is quite similar to that of NH<sub>2</sub>D; therefore, we only briefly recall the key aspects and highlight the major differences.

Doubly-deuterated ammonia is an asymmetric-top rotor with a double-minima potential energy surface. The tunneling between the two equivalent configurations splits each  $J_{K_a, K_c}$  rotational level into two sub-levels, one symmetric (*s*) and one anti-symmetric (*a*) with respect to inversion. As in the case of NH<sub>2</sub>D, the inversion motion of ND<sub>2</sub>H occurs along the *c*-axis; however, the *a*- and *b*-axes are reversed. Hence, the spectrum of ND<sub>2</sub>H is characterized by weak *b*-type transitions within each sub-state and stronger *c*-type transitions connecting the two inversion states [28].

All nuclei present in the molecule having nonzero nuclear spins contribute to the hyperfine structure of the rotational spectrum of ND<sub>2</sub>H. The HFS is dominated by the nuclear quadrupole coupling (NQC) of nitrogen, but spin-rotation (SR) interactions as well as NQC effects due to the deuterium nuclei have an appreciable impact on it. Moreover, the presence of two equivalent D nuclei leads to the existence of *ortho* and *para* species, and the total nuclear spin  $I_{D, \text{tot}} = I_{D_1} + I_{D_2}$  must be taken into account. The *ortho* species corresponds to  $I_{D, \text{tot}} = 0$  or 2, whereas the *para* form is characterized by  $I_{D, \text{tot}} = 1$ . This results in an *ortho:para* spin-statistical weight ratio of 2:1. Since the two equivalent particles are bosons, the Bose-Einstein statistics holds. Given that the total wavefunction has to be symmetric with the respect to the exchange of the two D nuclei, the *ortho* form has rotation-inversion states of the type (*s, ee*), (*s, oo*), (*a, eo*), and (*a, oe*), while the *para* species possesses (*s, eo*), (*s, oe*), (*a, ee*), and (*a, oo*) states.

While the Hamiltonian used in the present analysis is identical to the one described in **Paper I**, the angular momentum coupling scheme adopted for the labelling of energy levels is slightly different:

$$\begin{aligned} \mathbf{F}_1 &= \mathbf{J} + \mathbf{I}_N, \\ \mathbf{F}_2 &= \mathbf{F}_1 + \mathbf{I}_{D, \text{tot}}, \\ \mathbf{F} &= \mathbf{F}_2 + \mathbf{I}_H, \end{aligned} \quad (1)$$

because of the presence of the two identical deuterium nuclei and only one hydrogen.

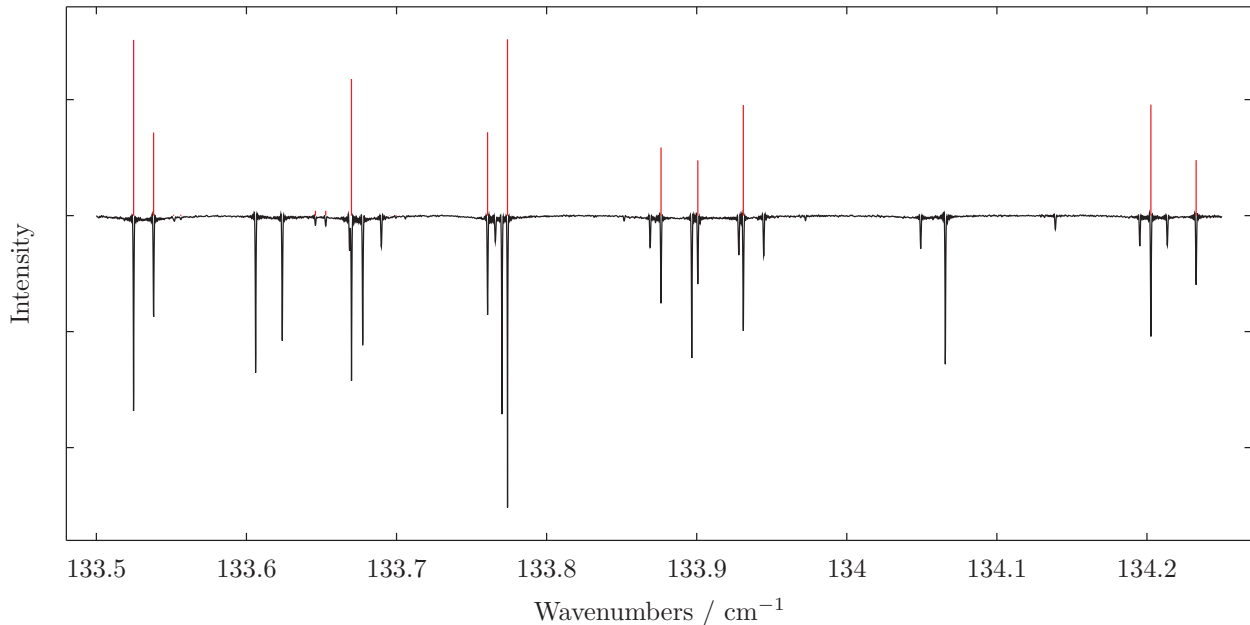


Figure 1: Portion of the FIR spectrum of  $\text{ND}_2\text{H}$  (black trace). The red bars indicate the position and intensity of some  $c$ -type R branch transitions, as predicted using the spectroscopic constants determined in this work. The remaining spectral lines belong to  $\text{ND}_3$  or to other by-products of the discharge. The intensity on the  $y$ -axis is expressed in arbitrary units.

### 3. Experiment

Rotational transitions of singly- and doubly-deuterated ammonia were recorded in the range 265–1565 GHz with a frequency-modulation sub-millimeter spectrometer [29]. The radiation source of the spectrometer is constituted by a series of Gunn diodes emitting between 80 and 134 GHz, which can be coupled with passive frequency multipliers (doublers and triplers). Terahertz frequencies are obtained by connecting two triplers in cascade guided by Gunn diodes working in the F band (115–134 GHz) [30, 31]. However, the twelfth harmonic of their radiation remains detectable with a power around few tens of  $\mu\text{W}$ , thus enabling to reach frequencies up to 1.6 THz. The radiation source is phase-locked to a harmonic of a centimeter-wave synthesizer (2–18 GHz), frequency modulated at  $f = 1 - 48$  kHz, and referenced to a 5 MHz rubidium atomic clock. The measurements were performed in a 3 m long glass absorption cell with the optical elements of the spectrometer arranged to perform, whenever possible, Lamb-dip measurements (for further details about the set-up, see **Paper I** as well as Refs. [32, 33, 34]). The output radiation was then detected by a liquid helium-cooled InSb bolometer and sent to a lock-in amplifier, set at twice the modulation frequency ( $2f$

detection scheme). Here, the sample of  $\text{NH}_2\text{D}$  was produced using the same methodology employed in **Paper I** (a small flow of  $\text{NH}_3$  in a cell where  $\text{D}_2$  had been previously discharged), whereas a good yield of  $\text{ND}_2\text{H}$  was obtained by flowing simply  $\text{ND}_3$  into the absorption cell.

Additional transitions in the range 45–220  $\text{cm}^{-1}$  were observed at the SOLEIL synchrotron using a Bruker IFS125HR FTIR interferometer, whose source is the bright synchrotron radiation extracted by the AILES beamline. The far-infrared (FIR) spectrum was recorded at a resolution of 0.001  $\text{cm}^{-1}$ , using the same set-up described in detail in Refs. [35, 36], during a measurement campaign of the  $\text{ND}_2$  radical. Although the experimental conditions were not optimized to form deuterated isotopologues of ammonia, the use of  $\text{ND}_3$  as precursor in a radio-frequency discharge produced strong –but not saturating– lines of  $\text{ND}_2\text{H}$  in the spectrum, as can be seen in Figure 1. Conversely,  $\text{NH}_2\text{D}$  seems to be much less abundant and only a few absorption lines were detected; therefore, its FIR spectrum could not be analyzed.

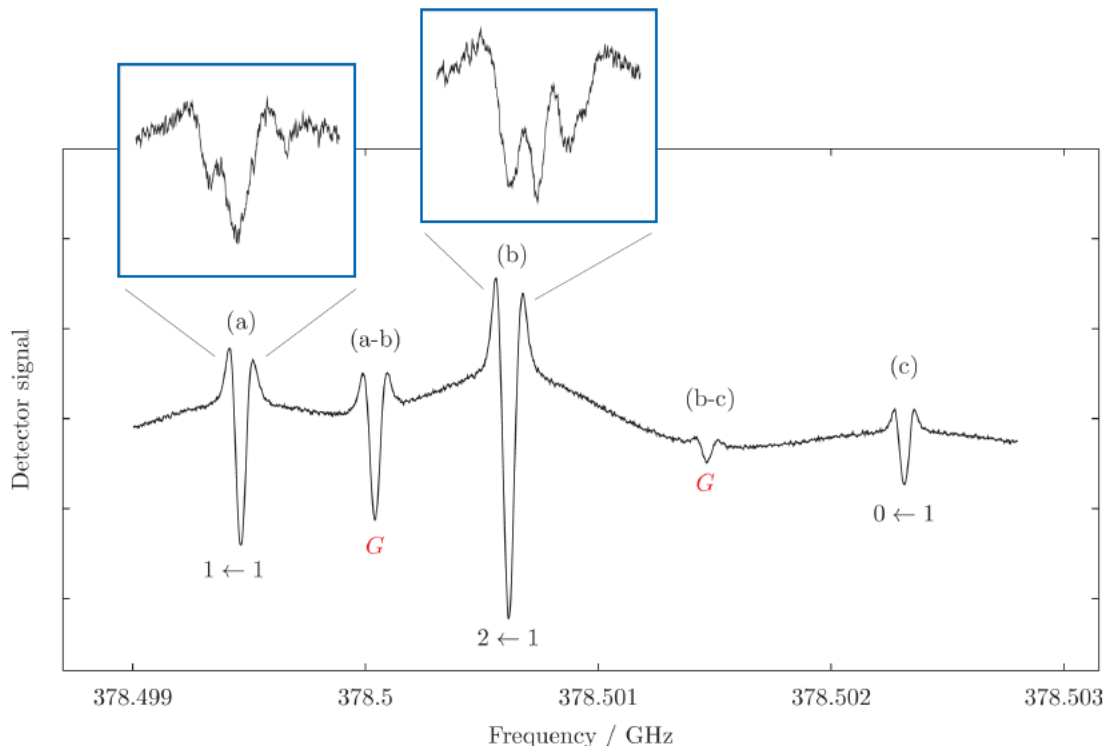


Figure 2: Lamb-dip spectrum of the  $J_{K_a, K_c} = 1_{1,0}^{(s)} - 0_{0,0}^{(a)}$   $p$ -ND<sub>2</sub>H transition. The numbers below each HFS components refer to the  $F_1' \leftarrow F_1$  quantum numbers, while a red  $G$  indicates a ghost feature. The labels above each line are used to denote the “interacting” transition frequencies from which the ghost transitions arise. The magnified boxes show the splittings due to deuterium quadrupolar interaction, as observed at higher-resolution experimental conditions. The vertical scale of the plots represents the detector response in arbitrary units.

## 4. Results

### 4.1. Spectral analysis

The latest sets of spectroscopic constants for NH<sub>2</sub>D and ND<sub>2</sub>H were retrieved from Paper I and the Cologne Database for Molecular Spectroscopy (CDMS) [37], respectively. The quality of these parameters was sufficient to search and assign rotational transitions from the submillimeter-wave (submm) to the far-infrared domain. Moreover, in order to correctly interpret the hyperfine structure of the ND<sub>2</sub>H spectrum, the NQC, SR, and dipolar spin-spin (SS) tensors of doubly-deuterated ammonia were computed using the approach described in Paper I.

Briefly, the equilibrium values of the hyperfine constants were computed using the CCSD(T) method [38] in conjunction with a series of correlation-consistent  $n$ -uple-zeta basis sets [39, 40, 41, 42, 43] (with  $n = Q, 5, 6$ ), correlating all electrons, and extrapolated to the complete basis set (CBS) limit. Then, exploiting the additiv-

ity approximation [44], the contributions due to the full treatment of triple and quadruple excitations were also taken into account using triple- and double-zeta basis sets, respectively. Subsequently, the equilibrium hyperfine parameters were augmented by the corresponding vibrational corrections in order to estimate the vibrational ground-state values. These corrections have been evaluated within the second-order vibrational perturbation theory (VPT2) [45] at the CCSD(T)/aug-cc-pCVQZ level of theory (with all electrons correlated). All CCSD(T) computations have been performed using the CFOUR package [46, 47], while the MRCC program [48, 49] interfaced to CFOUR has been employed for CCSDT and CCSDTQ calculations. The computed values of all NQC, SR, and SS interaction constants are listed in Table 1. According to the literature on this topic (see, e.g., Refs. [27, 32, 50]), the computational methodology employed is able to provide quantitative predictions of hyperfine parameters. In more detail, for nuclear

209 quadrupole coupling constants, the discrepancy be- 222  
 210 tween experimental and computed values is below 223  
 211 20 kHz for parameters as small as those encountered 224  
 212 in this work. Moving to nuclear spin-rotation con- 225  
 213 stants, discrepancies usually range from hundredths 226  
 214 of kHz to a few kHz.

Table 1: Computed nuclear quadrupole, spin-rotation, and dipolar spin-spin coupling constants of ND<sub>2</sub>H.

Constant	Atom	Unit	ND <sub>2</sub> H
$\chi_{aa}$	(N)	MHz	-2.048
$\chi_{cc}$	(N)	MHz	-3.842
$C_{aa}$	(N)	kHz	5.229
$C_{bb}$	(N)	kHz	3.756
$C_{cc}$	(N)	kHz	4.000
$\chi_{aa}$	(D)	MHz	0.135
$\chi_{cc}$	(D)	MHz	-0.124
$C_{aa}$	(D)	kHz	-1.228
$C_{bb}$	(D)	kHz	-1.888
$C_{cc}$	(D)	kHz	-1.860
$C_{aa}$	(H)	kHz	-23.595
$C_{bb}$	(H)	kHz	-5.058
$C_{cc}$	(H)	kHz	-9.115
$D_{bb}$	(N-D)	kHz	0.19
$D_{cc}$	(N-D)	kHz	0.98
$D_{bb}$	(N-H)	kHz	-8.62
$D_{cc}$	(N-H)	kHz	0.66
$D_{bb}$	(H-D)	kHz	-4.89
$D_{cc}$	(H-D)	kHz	3.82
$D_{bb}$	(D-D)	kHz	0.65
$D_{cc}$	(D-D)	kHz	0.65

**Notes:** The nuclear quadrupole ( $\chi_{ii}$ ) and dipolar spin-spin coupling ( $D_{ii}$ ) tensors have zero trace; therefore, only two of the three diagonal components are given.

215 For the first time, the complex hyperfine 261  
 216 structure caused by the nitrogen and deuterium 262  
 217 quadrupole couplings has been revealed in some low 263  
 218  $J$  transitions of ND<sub>2</sub>H. As an example, Figure 2 264  
 219 shows the Lamb-dip spectrum of the fundamen- 265  
 220 tal  $c$ -type rotation-inversion transition  $J_{K_a, K_c} =$  266  
 221  $1_{1,0}^{(s)} - 0_{0,0}^{(a)}$  of the *para* species. The main panel illus-

222 trates the three  $F_1$  components ( $\Delta F_1 = 0, \pm 1$ ) and 223  
 224 two ghost transitions<sup>1</sup> (marked with a red  $G$ ) oc- 225  
 226 ccurring in between, while the magnified boxes high- 227  
 228 light the deuterium HF splittings corresponding to 229  
 230 different  $F'_2 - F_2$  components. A similar resolution 231  
 232 has been obtained also for the  $J_{K_a, K_c} = 1_{1,0}^{(a)} - 0_{0,0}^{(s)}$  233  
 234 transition of *o*-ND<sub>2</sub>H.

235 Additional measurements of NH<sub>2</sub>D and ND<sub>2</sub>H 236  
 237 were performed with three main aims: (i) to re- 238  
 239 solve the HFS as much as possible for those tran- 240  
 241 sitions which can be used in astronomical observa- 242  
 243 tions (typically involving low-energy levels), (ii) to 244  
 245 exploit the Lamb-dip technique at THz frequencies 246  
 247 in order to achieve an accuracy of about 10 ppb 248  
 249 on the line position, and (iii) to revise the submm 249  
 250 and FIR spectra at higher resolution. In particu- 251  
 252 lar, we have observed about one hundred transi- 253  
 254 tions of NH<sub>2</sub>D and ND<sub>2</sub>H in the mm/submm re- 255  
 256 gion, half of which show the HFS at least partially 256  
 257 resolved. For ND<sub>2</sub>H only, we also detected and an- 257  
 258 alyzed more than 700 distinct FIR transitions in- 258  
 259 volving rotation-inversion levels with  $J$  up to 18.

260 The newly measured data were collected together 261  
 262 with all pure-rotational literature data [51, 52, 53, 262  
 263 54, 55, 28, 27] and processed into a combined anal- 263  
 264 ysis. A least-squares procedure was performed 264  
 265 with the SPFIT subroutine of the CALPGM program 265  
 266 suite [56], where each datum is weighted propor- 266  
 267 tionally to the inverse square of its uncertainty. 267  
 268 The error associated to our line positions is in the 268  
 269 range 2–100 kHz for mm/submm transitions and 269  
 270  $5 \times 10^{-5} \text{ cm}^{-1}$  for FIR lines, while literature data 270  
 271 were used with their declared uncertainty. **Unre-** 271  
 272 **solved lines were incorporated in the fit as intensity-** 272  
 273 **weighted average of the individual components in-** 273  
 274 **olved in the blended feature, as implemented in** 274  
 275 **SPFIT.**

276 The fit results for NH<sub>2</sub>D and ND<sub>2</sub>H have sim- 276  
 277 ilar quality, despite the different number of avail- 277  
 278 able data. The overall fit standard deviation ( $\sigma$ ) is 278  
 279 close to 1 in both cases and the root-mean-square 279  
 280 (rms) error is below 100 kHz for mm/submm data 280  
 281 and around  $0.0002 \text{ cm}^{-1}$  for the FIR transitions. 281  
 282 These values indicate that the modeling of both 282  
 283 species is satisfactory and can be used to generate 283  
 284 spectral predictions in a wide range of frequencies 284  
 285

<sup>1</sup>Ghost transitions, also denoted as crossover resonances, are due to the saturation of overlapping Gaussian profiles of two transitions sharing a common energy level. They occur at the arithmetic mean frequency of the overlapping transitions.

with a low uncertainty. The derived rotational and centrifugal distortion constants, Coriolis interaction terms, and HFS parameters are given in Tables 2–4. All parameters have been improved, with respect to previous studies, by up to one order of magnitude. Moreover, the ND<sub>2</sub>H quadrupole coupling constant  $\chi_{cc}(\text{D})$  has been determined for the first time and allows the simulation of the deuterium HFS. Its derived value, -0.121(4), agrees very well with the computed counterpart, -0.124. Instead, the hydrogen HFS could not be resolved in the laboratory spectra, thus preventing the experimental determination of the hydrogen spin-rotation constants. Simulations based on the calculated parameters showed that the hydrogen HFS is so small that it does not affect the spectral linewidths.

The SPFIT input files (.PAR and .LIN) as well as a re-formatted version of the .FIT output file are provided for both species as Supplementary Material.

#### 4.2. Line catalogs for astronomical purposes

In order to produce meaningful line lists that can be used for astronomical observations of NH<sub>2</sub>D and ND<sub>2</sub>H, the new sets of spectroscopic constants must be combined with accurate estimates of the rotational partition function ( $Q_{\text{rot}}$ ) and dipole moment components. The latter were evaluated in Refs. [54] and [28] and are:  $\mu_a = -0.185$  D and  $\mu_c = 1.46$  D for NH<sub>2</sub>D and  $\mu_b = 0.21$  D and  $\mu_c = 1.47$  D for ND<sub>2</sub>H.

The rotational partition functions, instead, have been calculated numerically using the SPCAT subroutine of the CALPGM suite [56]. The temperature dependence of  $Q_{\text{rot}}$  was computed separately for the *ortho* and *para* species at three different “resolutions”: (i) without the inclusion of any HFS, (ii) considering only the contribution of nitrogen, and (iii) including the effects of both N and D nuclei. These distinctions have been made in order to support the analysis of interstellar deuterated ammonia at different spectral resolution. Moreover, at the low temperatures of cold molecular clouds (5–10 K), the *ortho* and *para* species must be treated as separate species. The rotational partition function values computed at temperatures between 2.725 and 300 K are provided as Supplementary Material.

#### 4.3. Application to L1544 starless core spectrum

To test the effect of the inclusion of D hyperfine structure in the analysis of astrophysical NH<sub>2</sub>D

Table 2: Ground-state rotational and centrifugal distortion constants up to the sixth power of the angular momentum.

Constant <sup>(a)</sup>	Unit	NH <sub>2</sub> D	ND <sub>2</sub> H
$\Delta E$	MHz	12169.466(1)	5118.8865(8)
$A$	MHz	290074.6(2)	223187.715(1)
$\Delta A$	MHz	-46.9120(8)	-16.1290(6)
$B$	MHz	192176.4768(8)	160214.998(4)
$\Delta B$	MHz	-17.34(2)	-5.3284(4)
$C$	MHz	140810.2(2)	112520.741(4)
$\Delta C$	MHz	11.2003(1)	4.0868(4)
$D_J$	MHz	15.7199(1)	3.5183(2)
$\Delta D_J$	MHz	-0.09412(4)	-0.000896(5)
$D_{JK}$	MHz	-23.7516(2)	-2.9356(9)
$\Delta D_{JK}$	MHz	0.19484(9)	-0.01008(3)
$D_K$	MHz	10.8484(3)	19.2808(7)
$\Delta D_K$	MHz	-0.10982(6)	-0.04472(5)
$d_1$	MHz	4.14089(8)	-1.2318(2)
$\Delta d_1$	MHz	-0.04166(4)	0.000795(4)
$d_2$	MHz	0.13787(4)	-0.28029(7)
$\Delta d_2$	MHz	0.00567(3)	0.001787(2)
$H_J$	kHz	3.537(3)	0.3353(9)
$\Delta H_J$	kHz	-0.1940(5)	0.00160(5)
$H_{JK}$	kHz	-8.422(4)	-1.21(1)
$\Delta H_{JK}$	kHz	0.4048(8)	-0.0055(2)
$H_{KJ}$	kHz	8.776(7)	2.16(4)
$\Delta H_{KJ}$	kHz	-0.3824(9)	-0.049(1)
$H_K$	kHz	-3.705(8)	4.75(3)
$\Delta H_K$	kHz	0.1762(4)	-0.089(1)
$h_1$	kHz	-1.832(3)	0.247(1)
$\Delta h_1$	kHz	0.1097(6)	-0.00060(3)
$h_2$	kHz	0.445(2)	0.0382(5)
$\Delta h_2$	kHz	-0.0146(6)	-0.00160(2)
$h_3$	kHz	-0.0403(5)	0.0225(2)
$\Delta h_3$	Hz	-0.0086(3)	-0.00097(1)

**Notes:** Numbers in parentheses are standard errors and apply to the last significant digits. <sup>(a)</sup> For a given parameter  $X$ ,  $\Delta X = (X^{(a)} - X^{(s)})/2$ .

emissions at millimeter wavelengths, we have used recent observations of the starless core L1544, a low-mass star-forming core in a very early stage of evolution. This source is a prototypical cold, quiescent core on the verge of the gravitational collapse, which exhibits very narrow line emissions due its low central temperature, subsonic contraction motion, and low turbulence [57, 58]. It also shows a high degree of deuteration [e.g., Ref. 59]) which



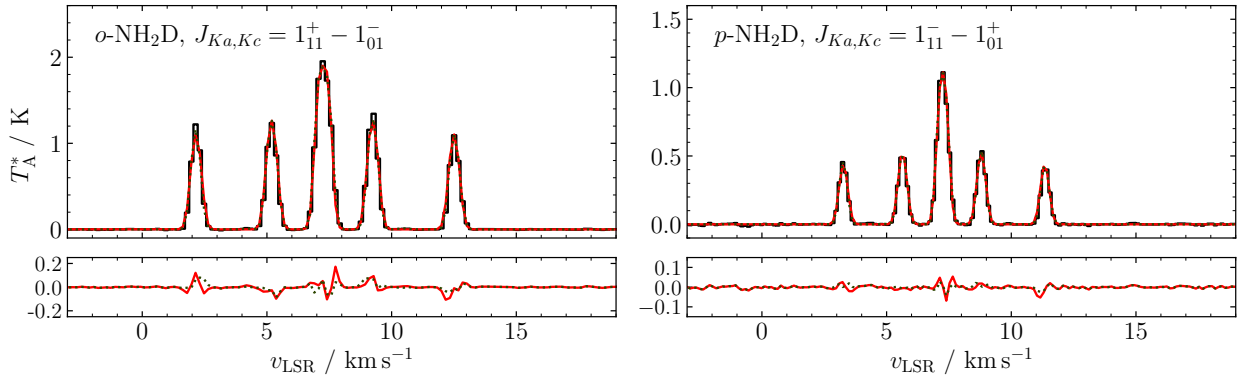


Figure 3: Spectra of the NH<sub>2</sub>D transitions observed towards L1544. (*Top left panel*):  $J_{K_a, K_c} = 1_{1,1}^{(s)} - 1_{0,1}^{(a)}$  *ortho* line at 85926.3 MHz. (*Top right panel*):  $J_{K_a, K_c} = 1_{1,1}^{(a)} - 1_{0,1}^{(s)}$  *para* line at 110153.6 MHz. The dotted green trace plots the model computed considering the full HFS (N+D). The solid red trace plots the model computed with the N quadrupole only. (*Bottom panels*): Residuals of both models, plotted using the same colour legend.

326 makes it an ideal astrophysical laboratory to observe 327  
 328 D-containing molecules and to reveal subtle 329  
 330 spectral effects due to the contribution of the deu- 331  
 332 terium quadrupole splittings. 332

333 The astronomical data used here were collected 334  
 335 using the IRAM 30m telescope (Pico Veleta, Spain) 336  
 337 in the past few years by some members of our team. 338  
 339 They were observed as part of the projects 008- 340  
 341 12, 013-13 (PI S. Spezzano) and 150-11, 127-12 342  
 343 (PI L. Bizzocchi). The observing runs were per- 344  
 345 formed in several sessions from May 2012 to Oc- 346  
 347 tober 2013. The frequency intervals of interest 348  
 349 have been extracted from the output of the wide- 350  
 351 band FTS spectrometer which was connected to the 352  
 353 3 mm band of the EMIR heterodyne receiver. The 354  
 355 *o*-NH<sub>2</sub>D lines at 85926.3 MHz and the ones of *p*- 356  
 357 NH<sub>2</sub>D at 110153.6 MHz were observed in the lower- 358  
 359 outer (LO) and upper-inner (UI) sub-band, respec- 360  
 361 tively. A detailed description of the observation 362  
 363 strategy and the data reduction can be found else- 364  
 365 where [60, 61, 62]. 366

367 The resulting spectra are shown in the two panels 368  
 369 of Figure 3, plotted as black histograms. Note that 370  
 371 the *x*-axis is labelled in radial equivalent velocity 372  
 373 using the rest frequency of the corresponding un- 374  
 375 splitted lines as reference. The solid red lines plot 376  
 377 the best fit model computed using the full HFS (in- 378  
 379 cluding D). The fitting was performed using a cus- 380  
 381 tom Python3 code described in Ref. [12]. The free 382  
 383 parameters of the optimisation are the column den- 384  
 385 sity ( $N$ ), the excitation temperature ( $T_{\text{ex}}$ ), the sys- 386  
 387 temic velocity ( $v_{\text{LSR}}$ ) and the line full-width-half- 388  
 389 maximum (FWHM), while the total opacity of the

379 transition ( $\tau$ ) is regarded as a derived quantity.

380 Table 5 collects the fit results of two different 381  
 382 analyses obtained by taking into account the nitro- 383  
 384 gen quadrupole coupling only (column labelled by 385  
 386 N) or the full hyperfine structure including the deu- 387  
 388 terium effects (N+D). While the two models would 389  
 390 be virtually indistinguishable by visual inspection, 391  
 392 small but significant differences are highlighted by 393  
 394 the fit results. Apart from a 30-40% reduction of 395  
 396 the residual rms, the proper treatment of the hy- 397  
 398 perfine effects entails a reduction of the derived line 399  
 400 FWHM of about 12%. This change is reflected by 401  
 402 the values of the related parameter  $N$  and  $T_{\text{ex}}$ , and 403  
 404 of the derived quantity  $\tau$ . For the less opaque emis- 405  
 406 sion (*p*-NH<sub>2</sub>D), the column density and the exci- 407  
 408 tation temperature readjust, while  $\tau$  remains sub- 409  
 410 stantially unchanged. For the thicker *o*-NH<sub>2</sub>D line, 411  
 412 the  $T_{\text{ex}}$  is unaffected and the deviation is mainly 413  
 414 observed by a relevant change of  $\tau$ . 415

## 378 5. Conclusions

379 The rotational spectra of singly- and doubly- 380  
 381 deuterated ammonia have been thoroughly re- 382  
 383 investigated at higher resolution. By means of the 384  
 385 Lamb-dip technique at submillimeter wavelengths 386  
 387 and with the use of synchrotron radiation in the 388  
 389 FIR region, a large number of transitions have been 390  
 391 measured with high accuracy. For some of them, 392  
 393 the nitrogen and deuterium hyperfine structure due 394  
 395 to electric and magnetic interactions has been un- 396  
 397 veiled, thus allowing the precise determination of

Table 3: Higher-order centrifugal distortion constants and Coriolis interaction parameters.

Constant <sup>(a)</sup>	Unit	NH <sub>2</sub> D	ND <sub>2</sub> H
$L_J$	Hz	-1.14(2)	
$\Delta L_J$	mHz	181.(2)	-3.7(1)
$L_{JJK}$	Hz	3.27(2)	-0.123(5)
$\Delta L_{JJK}$	Hz	-0.468(5)	
$L_{JK}$	Hz	-5.63(7)	-0.50(4)
$\Delta L_{JK}$	Hz	0.711(8)	
$L_{KKJ}$	Hz	5.1(1)	1.4(1)
$\Delta L_{KKJ}$	Hz	-0.729(6)	0.30(1)
$L_K$	Hz	-2.1(1)	-3.60(6)
$\Delta L_K$	Hz	0.306(2)	-0.026(6)
$l_1$	Hz	0.80(2)	0.080(3)
$\Delta l_1$	mHz	-22.(2)	0.38(5)
$l_2$	Hz	-0.30(1)	-0.0185(3)
$\Delta l_2$	mHz	-152.(6)	1.98(6)
$l_3$	mHz	18.(3)	-4.7(2)
$\Delta l_3$	mHz	112.(5)	0.14(5)
$l_4$	mHz		-1.55(6)
$\Delta l_4$	mHz	-22.(1)	0.48(1)
$M_{KKJ}$	mHz		1.35(3)
$M_K$	mHz	1.3(3)	1.35(3)
$F_{ij}$	MHz	-5097.(3)	3129.49(4)
$F_{ij}^J$	MHz		0.812(3)
$F_{ij}^K$	MHz		-9.00(2)
$F_{ij}^{JJ}$	kHz		-1.49(2)
$F_{ij}^{JK}$	kHz		4.4(1)
$F_{ij}^{KK}$	kHz		9.8(4)
$F_{ij}^{JJJ}$	Hz		-1.22(4)

**Notes:** Numbers in parentheses are standard errors and apply to the last significant digits. <sup>(a)</sup> For a given parameter  $X$ ,  $\Delta X = (X^{(a)} - X^{(s)})/2$ .  $F_{ij}$  corresponds to  $F_{ab}$  and  $F_{bc}$  for NH<sub>2</sub>D and ND<sub>2</sub>H, respectively.

nuclear quadrupole coupling and spin-rotation constants. Moreover, all the values of rotational and centrifugal distortion parameters could be refined thanks to the analysis of an extended dataset.

The new set of spectroscopic constants has been then used to evaluate the impact of the deuterium HFS on the analysis of astrophysical NH<sub>2</sub>D lines towards L1544. The narrow line emissions of this pre-stellar core made it possible to detect small but significant differences in the physical parameters determined when both nitrogen and deuterium hyperfine interactions are taken into account. In addition

Table 4: Nitrogen and deuterium hyperfine constants (only the parameters used in the analyses are listed).

Constant	Atom	Unit	NH <sub>2</sub> D	ND <sub>2</sub> H
$\chi_{aa}$	(N)	MHz	1.909(3)	-2.038(8)
$\chi_{cc}$	(N)	MHz	-3.948(1)	-3.852(2)
$C_{aa}$	(N)	kHz	6.1(8)	5.229
$C_{bb}$	(N)	kHz	3.8(7)	3.756
$C_{cc}$	(N)	kHz	5.1(2)	4.000
$\chi_{aa}$	(D)	MHz	0.225(5)	0.132
$\chi_{cc}$	(D)	MHz	-0.135(1)	-0.121(4)
$C_{aa}$	(D)	kHz	-0.125	-1.228
$C_{bb}$	(D)	kHz	-3.154	-1.888
$C_{cc}$	(D)	kHz	-2.27(9)	-1.860

**Notes:** Numbers within parentheses are the standard errors and apply to the last significant digits. Non-determinable parameters (values given without error) have been kept fixed at the corresponding computed values (see Table 1).

to the improvement of the fit results in term of rms residual, the observed reduction of the line FWHM produces a change in the determination of the column density of *ortho*- and *para*-NH<sub>2</sub>D of about 5–20 %. This observation demonstrates the importance of modelling all the effects that can contribute to the determination of molecular abundances for interstellar species.

## 6. Supplementary Material Available

The file “partition-function-values.pdf” contains the rotational partition function values computed at temperatures between 2.725 and 300 K for the *ortho* and *para* species of ND<sub>2</sub>H and NH<sub>2</sub>D. The files “nh2d.lin”, “nh2d.par”, “nd2h.lin”, and “nd2h.par” are the SPFIT input files used in our analysis. The files “nh2d\_reformatted.out” and “nd2h\_reformatted.out” are a reformatted version of the SPFIT output files.

## 7. Acknowledgement

This study was supported by Bologna University (RFO funds) and by MIUR (Project PRIN 2015: STARS in the CAOS, Grant Number 2015F59J3R), and in Mainz by the Deutsche Forschungsgemeinschaft via grant GA 370/6-2. Part of the measurements has been performed under the SOLEIL

Table 5: Analysis of the ortho and para NH<sub>2</sub>D emissions in L1544 considering nitrogen quadrupole coupling only (N) or the full hyperfine structure (N+D).

Parameter	Unit	<i>o</i> -NH <sub>2</sub> D		<i>p</i> -NH <sub>2</sub> D	
		N	N+D	N	N+D
$N$	10 <sup>14</sup> cm <sup>-2</sup>	5.92(20)	5.64(15)	3.01(14)	2.44(9)
$T_{\text{ex}}$	K	4.46(2)	4.47(2)	3.95(3)	4.07(2)
$v_{\text{LSR}}$	km s <sup>-1</sup>	7.265(2)	7.265(2)	7.194(1)	7.195(1)
FWHM	km s <sup>-1</sup>	0.444(3)	0.388(3)	0.389(3)	0.346(2)
$\tau^a$		7.47	8.22	3.48	3.46
rms <sup>b</sup>	mK	56	39	19	11

**Notes:** Numbers within parentheses are the standard errors and apply to the last significant digits. <sup>a</sup> Derived quantity. <sup>b</sup> Root-mean-square of the residuals computed on lines.

426 proposal #20110017; we acknowledge the SOLEIL 462  
427 facility for provision of synchrotron radiation and 463  
428 would like to thank the AILES beamline staff for 464  
429 their assistance and in particular Dr. M.-A. Martin- 465  
430 Drumel and Dr. O. Pirali for their help during the 466  
431 spectral recording. L.B., S.S, and P.C. acknowl- 467  
432 edge the support by the Max Planck Society. N.J. 468  
433 thanks the China Scholarships Council (CSC) for 469  
434 the financial support. 470

## 435 References

436 [1] B. A. McGuire, 2018 Census of Interstellar, Circumstel- 477  
437 lar, Extragalactic, Protoplanetary Disk, and Exoplanetary 478  
438 Molecules, *Astrophys. J. Suppl. S.* 239 (2018) 17. 479  
439 [2] A. López-Sepulcre, N. Balucani, C. Ceccarelli, 480  
440 C. Codella, F. Dulieu, P. Theulé, Interstellar formamide 481  
441 (NH<sub>2</sub>CHO), a key prebiotic precursor, *ACS Earth* 482  
442 *Space Chem.* 3 (10) (2019) 2122–2137. 483  
443 [3] V. M. Rivilla, J. Martín-Pintado, I. Jiménez-Serra, 484  
444 S. Martín, L. F. Rodríguez-Almeida, M. A. Requena- 485  
445 Torres, et al., Prebiotic precursors of the primordial 486  
446 RNA world in space: Detection of NH<sub>2</sub>OH, *Astrophys.* 487  
447 *J. Lett.* 899 (2) (2020) L28. 488  
448 [4] S. A. Sandford, M. Nuevo, P. P. Bera, T. J. Lee, Pre- 489  
449 biotic astrochemistry and the formation of molecules of 490  
450 astrobiological interest in interstellar clouds and proto- 491  
451 stellar disks, *Chem. Rev.* 492  
452 [5] Y.-J. Kuan, S. B. Charnley, H.-C. Huang, W.-L. Tseng, 493  
453 Z. Kisiel, Interstellar glycine, *Astrophys. J.* 593 (2) 494  
454 (2003) 848. 495  
455 [6] L. E. Snyder, F. J. Lovas, J. M. Hollis, D. N. Friedel, 496  
456 P. R. Jewell, A. Remijan, et al., A rigorous attempt to 497  
457 verify interstellar glycine, *Astrophys. J.* 619 (2) (2005) 498  
458 914–930. doi:10.1086/426677. 499  
459 URL <https://doi.org/10.1086/426677> 500  
460 [7] M. Melosso, B. A. McGuire, F. Tamassia, C. Degli Es- 501  
461 posti, L. Dore, Astronomical search of vinyl alcohol as-

502 503  
504 505  
506 507  
508 509  
510 511  
512 513  
514 515  
516 517  
518 519  
519 520  
521 522  
523 524  
525 526  
527 528  
529 530  
531 532  
533 534  
535 536  
537 538  
539 540  
541 542  
543 544  
545 546  
547 548  
549 550  
551 552  
553 554  
555 556  
557 558  
559 560  
561 562  
563 564  
565 566  
567 568  
569 570  
571 572  
573 574  
575 576  
577 578  
579 580  
581 582  
583 584  
585 586  
587 588  
589 590  
591 592  
593 594  
595 596  
597 598  
599 600  
601 602  
603 604  
605 606  
607 608  
609 610  
611 612  
613 614  
615 616  
617 618  
619 620  
621 622  
623 624  
625 626  
627 628  
629 630  
631 632  
633 634  
635 636  
637 638  
639 640  
641 642  
643 644  
645 646  
647 648  
649 649  
650 651  
651 652  
652 653  
653 654  
654 655  
655 656  
656 657  
657 658  
658 659  
659 660  
660 661  
661 662  
662 663  
663 664  
664 665  
665 666  
666 667  
667 668  
668 669  
669 670  
670 671  
671 672  
672 673  
673 674  
674 675  
675 676  
676 677  
677 678  
678 679  
679 680  
680 681  
681 682  
682 683  
683 684  
684 685  
685 686  
686 687  
687 688  
688 689  
689 690  
690 691  
691 692  
692 693  
693 694  
694 695  
695 696  
696 697  
697 698  
698 699  
699 700  
700 701  
701 702  
702 703  
703 704  
704 705  
705 706  
706 707  
707 708  
708 709  
709 710  
710 711  
711 712  
712 713  
713 714  
714 715  
715 716  
716 717  
717 718  
718 719  
719 720  
720 721  
721 722  
722 723  
723 724  
724 725  
725 726  
726 727  
727 728  
728 729  
729 730  
730 731  
731 732  
732 733  
733 734  
734 735  
735 736  
736 737  
737 738  
738 739  
739 740  
740 741  
741 742  
742 743  
743 744  
744 745  
745 746  
746 747  
747 748  
748 749  
749 750  
750 751  
751 752  
752 753  
753 754  
754 755  
755 756  
756 757  
757 758  
758 759  
759 760  
760 761  
761 762  
762 763  
763 764  
764 765  
765 766  
766 767  
767 768  
768 769  
769 770  
770 771  
771 772  
772 773  
773 774  
774 775  
775 776  
776 777  
777 778  
778 779  
779 780  
780 781  
781 782  
782 783  
783 784  
784 785  
785 786  
786 787  
787 788  
788 789  
789 790  
790 791  
791 792  
792 793  
793 794  
794 795  
795 796  
796 797  
797 798  
798 799  
799 800  
800 801  
801 802  
802 803  
803 804  
804 805  
805 806  
806 807  
807 808  
808 809  
809 810  
810 811  
811 812  
812 813  
813 814  
814 815  
815 816  
816 817  
817 818  
818 819  
819 820  
820 821  
821 822  
822 823  
823 824  
824 825  
825 826  
826 827  
827 828  
828 829  
829 830  
830 831  
831 832  
832 833  
833 834  
834 835  
835 836  
836 837  
837 838  
838 839  
839 840  
840 841  
841 842  
842 843  
843 844  
844 845  
845 846  
846 847  
847 848  
848 849  
849 850  
850 851  
851 852  
852 853  
853 854  
854 855  
855 856  
856 857  
857 858  
858 859  
859 860  
860 861  
861 862  
862 863  
863 864  
864 865  
865 866  
866 867  
867 868  
868 869  
869 870  
870 871  
871 872  
872 873  
873 874  
874 875  
875 876  
876 877  
877 878  
878 879  
879 880  
880 881  
881 882  
882 883  
883 884  
884 885  
885 886  
886 887  
887 888  
888 889  
889 890  
890 891  
891 892  
892 893  
893 894  
894 895  
895 896  
896 897  
897 898  
898 899  
899 900  
900 901  
901 902  
902 903  
903 904  
904 905  
905 906  
906 907  
907 908  
908 909  
909 910  
910 911  
911 912  
912 913  
913 914  
914 915  
915 916  
916 917  
917 918  
918 919  
919 920  
920 921  
921 922  
922 923  
923 924  
924 925  
925 926  
926 927  
927 928  
928 929  
929 930  
930 931  
931 932  
932 933  
933 934  
934 935  
935 936  
936 937  
937 938  
938 939  
939 940  
940 941  
941 942  
942 943  
943 944  
944 945  
945 946  
946 947  
947 948  
948 949  
949 950  
950 951  
951 952  
952 953  
953 954  
954 955  
955 956  
956 957  
957 958  
958 959  
959 960  
960 961  
961 962  
962 963  
963 964  
964 965  
965 966  
966 967  
967 968  
968 969  
969 970  
970 971  
971 972  
972 973  
973 974  
974 975  
975 976  
976 977  
977 978  
978 979  
979 980  
980 981  
981 982  
982 983  
983 984  
984 985  
985 986  
986 987  
987 988  
988 989  
989 990  
990 991  
991 992  
992 993  
993 994  
994 995  
995 996  
996 997  
997 998  
998 999  
999 1000

- Carthy, Detection of the aromatic molecule benzonitrile ( $c\text{-C}_6\text{H}_5\text{CN}$ ) in the interstellar medium, *Science* 359 (6372) (2018) 202–205.
- [17] A. Coletta, F. Fontani, V. Rivilla, C. Mininni, L. Colzi, Á. Sánchez-Monge, M. Beltrán, Evolutionary study of complex organic molecules in high-mass star-forming regions, *Astron. Astrophys.* 641 (2020) A54.
- [18] J. K. Jørgensen, A. Belloche, R. T. Garrod, Astrochemistry during the formation of stars, *Ann. Rev. Astron. Astrophys.* 58 (2020) 727–778.
- [19] P. Caselli, T. Hasegawa, E. Herbst, Chemical differentiation between star-forming regions—the orion hot core and compact ridge, *Astrophys. J.* 408 (1993) 548–558.
- [20] S. Spezzano, L. Bizzocchi, P. Caselli, J. Harju, S. Brünken, Chemical differentiation in a prestellar core traces non-uniform illumination, *Astron. Astrophys.* 592 (2016) L11.
- [21] Y. Aikawa, K. Furuya, S. Yamamoto, N. Sakai, Chemical variation among protostellar cores: Dependence on prestellar core conditions, *Astrophys. J.* 897 (2) (2020) 110.
- [22] L. Bizzocchi, F. Tamassia, J. Laas, B. M. Giuliano, C. Degli Esposti, L. Dore, et al., Rotational and high-resolution infrared spectrum of  $\text{HC}_3\text{N}$ : global rovibrational analysis and improved line catalog for astrophysical observations, *Astrophys. J. Suppl. S.* 233 (1) (2017) 11.
- [23] M. Melosso, A. Belloche, M.-A. Martin-Drumel, O. Pirali, F. Tamassia, L. Bizzocchi, et al., Far-infrared laboratory spectroscopy of aminoacetonitrile and first interstellar detection of its vibrationally excited transitions, *Astron. Astrophys.* 641 (2020) A160.
- [24] M. Carvajal, C. Favre, I. Kleiner, C. Ceccarelli, E. Bergin, D. Fedele, Impact of nonconvergence and various approximations of the partition function on the molecular column densities in the interstellar medium, *Astron. Astrophys.* 627 (2019) A65.
- [25] F. Daniel, L. Coudert, A. Punanova, J. Harju, A. Faure, E. Roueff, et al., The  $\text{NH}_2\text{D}$  hyperfine structure revealed by astrophysical observations, *Astron. Astrophys.* 586 (2016) L4.
- [26] J. Harju, F. Daniel, O. Sipilä, P. Caselli, J. E. Pineda, R. K. Friesen, et al., Deuteration of ammonia in the starless core Ophiuchus/H-MM1, *Astron. Astrophys.* 600 (2017) A61.
- [27] M. Melosso, L. Dore, J. Gauss, C. Puzzarini, Deuterium hyperfine splittings in the rotational spectrum of  $\text{NH}_2\text{D}$  as revealed by Lamb-dip spectroscopy, *J. Mol. Spectrosc.* (2020) 111291.
- [28] C. Endres, H. Müller, S. Brünken, D. Paveliev, T. Giesen, S. Schlemmer, F. Lewen, High resolution rotation–inversion spectroscopy on doubly deuterated ammonia,  $\text{ND}_2\text{H}$ , up to 2.6 THz, *J. Mol. Struct.* 795 (1–3) (2006) 242–255.
- [29] M. Melosso, L. Bizzocchi, F. Tamassia, C. Degli Esposti, E. Cané, L. Dore, The rotational spectrum of  $^{15}\text{ND}$ : isotopic-independent Dunham-type analysis of the imidogen radical, *Phys. Chem. Chem. Phys.* 21 (2019) 3564–3573.
- [30] M. Melosso, C. Degli Esposti, L. Dore, Terahertz spectroscopy and global analysis of the rotational spectrum of doubly deuterated amidogen radical  $\text{ND}_2$ , *Astrophys. J. Suppl. S.* 233 (1) (2017) 15.
- [31] M. Melosso, B. Conversazioni, C. Degli Esposti, L. Dore, E. Cané, F. Tamassia, L. Bizzocchi, The pure rotational spectrum of  $^{15}\text{ND}_2$  observed by millimetre and submillimetre-wave spectroscopy, *J. Quant. Spectrosc. Ra.* 222 (2019) 186–189.
- [32] C. Puzzarini, G. Cazzoli, M. E. Harding, J. Vázquez, J. Gauss, A new experimental absolute nuclear magnetic shielding scale for oxygen based on the rotational hyperfine structure of  $\text{H}^{17}_2\text{O}$ , *J. Chem. Phys.* 131 (2009) 234304.
- [33] C. Puzzarini, G. Cazzoli, M. E. Harding, J. Vázquez, J. Gauss, The hyperfine structure in the rotational spectra of  $\text{D}^{17}_2\text{O}$  and  $\text{HD}^{17}\text{O}$ : Confirmation of the absolute nuclear magnetic shielding scale for oxygen, *J. Chem. Phys.* 142 (2015) 124308.
- [34] L. Dore, L. Bizzocchi, C. Degli Esposti, J. Gauss, The magnetic hyperfine structure in the rotational spectrum of  $\text{H}_2\text{CNH}$ , *J. Mol. Spectrosc.* 263 (2010) 44–50.
- [35] L. Bizzocchi, M. Melosso, B. M. Giuliano, L. Dore, F. Tamassia, M.-A. Martin-Drumel, et al., Submillimeter and far-infrared spectroscopy of monodeuterated amidogen radical (NHD): Improved rest frequencies for astrophysical observations, *Astrophys. J. Suppl. S.* 247 (2) (2020) 59.
- [36] M. Melosso, L. Bizzocchi, A. Adamczyk, E. Cané, P. Caselli, L. Colzi, et al., Extensive ro-vibrational analysis of deuterated-cyanoacetylene ( $\text{DC}_3\text{N}$ ) from millimeter-wavelengths to the infrared domain, *J. Quant. Spectrosc. Ra.* 254 (2020) 107221.
- [37] H. S. Müller, F. Schlöder, J. Stutzki, G. Winnewisser, The cologne database for molecular spectroscopy, CDMS: a useful tool for astronomers and spectroscopists, *J. Mol. Struct.* 742 (1–3) (2005) 215–227.
- [38] K. Raghavachari, G. W. Trucks, J. A. Pople, M. Head-Gordon, A fifth-order perturbation comparison of electron correlation theories, *Chem. Phys. Lett.* 157 (1989) 479–483.
- [39] T. H. Dunning Jr., Gaussian Basis Sets for Use in Correlated Molecular Calculations. I. The Atoms Boron through Neon and Hydrogen, *J. Chem. Phys.* 90 (1989) 1007.
- [40] A. Kendall, T. H. Dunning Jr., R. J. Harrison, Electron affinities of the first-row atoms revisited. Systematic basis sets and wave functions, *J. Chem. Phys.* 96 (1992) 6796.
- [41] D. E. Woon, T. H. Dunning Jr., Gaussian basis sets for use in correlated molecular calculations. V. Core-valence basis sets for boron through neon, *J. Chem. Phys.* 103 (1995) 4572.
- [42] A. K. Wilson, T. van Mourik, T. H. Dunning Jr, Gaussian basis sets for use in correlated molecular calculations. VI. Sextuple zeta correlation consistent basis sets for boron through neon, *J. Mol. Struct. THEOCHEM* 388 (1996) 339–349.
- [43] T. Van Mourik, A. K. Wilson, T. H. Dunning Jr, Benchmark calculations with correlated molecular wavefunctions. XIII. Potential energy curves for  $\text{He}_2$ ,  $\text{Ne}_2$  and  $\text{Ar}_2$  using correlation consistent basis sets through augmented sextuple zeta, *Mol. Phys.* 96 (1999) 529–547.
- [44] C. Puzzarini, M. Heckert, J. Gauss, The accuracy of rotational constants predicted by high-level quantum-chemical calculations. i. molecules containing first-row atoms, *J. Chem. Phys.* 128 (19) (2008) 194108.
- [45] I. M. Mills, Vibration-rotation structure in asymmetric and symmetric-top molecules, Vol. 1, 1972, p. 115.
- [46] J. F. Stanton, J. Gauss, L. Cheng, M. E. Harding, D. A. Matthews, P. G. Szalay, CFOUR, coupled-cluster

- 633 techniques for computational chemistry, a quantum- 698  
634 chemical program package, With contributions from 699  
635 A.A. Auer, R.J. Bartlett, U. Benedikt, C. Berger, 700  
636 D.E. Bernholdt, Y.J. Bomble, O. Christiansen, F. En- 701  
637 gel, R. Faber, M. Heckert, O. Heun, M. Hilgenberg, 702  
638 C. Huber, T.-C. Jagau, D. Jonsson, J. Jusélius, T. 703  
639 Kirsch, K. Klein, W.J. Lauderdale, F. Lipparini, T.  
640 Metzroth, L.A. Mück, D.P. O'Neill, D.R. Price, E.  
641 Prochnow, C. Puzzarini, K. Ruud, F. Schiffmann, W.  
642 Schwalbach, C. Simmons, S. Stopkowicz, A. Tajti, J.  
643 Vázquez, F. Wang, J.D. Watts and the integral pack-  
644 ages MOLECULE (J. Almlöf and P.R. Taylor), PROPS  
645 (P.R. Taylor), ABACUS (T. Helgaker, H.J. Aa. Jensen,  
646 P. Jørgensen, and J. Olsen), and ECP routines by A.  
647 V. Mitin and C. van Wüllen. For the current version,  
648 see <http://www.cfour.de>.
- [47] D. A. Matthews, L. Cheng, M. E. Harding, F. Lipparini,  
649 S. Stopkowicz, T.-C. Jagau, et al., Coupled-cluster tech-  
650 niques for computational chemistry: The cfour program  
651 package, *J. Chem. Phys.* 152 (21) (2020) 214108.
- [48] M. Kállay, MRCC, a generalized CC/CI program, For  
652 the current version, see <http://www.mrcc.hu>.
- [49] M. Kállay, P. R. Nagy, D. Mester, Z. Rolik, G. Samu,  
653 J. Csontos, et al., The mrcc program system: Accurate  
654 quantum chemistry from water to proteins, *J. Chem.*  
655 *Phys.* 152 (7) (2020) 074107.
- [50] T. Helgaker, J. Gauss, G. Cazzoli, C. Puzzarini,  $^{33}\text{S}$   
656 hyperfine interactions in  $\text{H}_2\text{S}$  and  $\text{SO}_2$  and revision of  
657 the sulfur nuclear magnetic shielding scale, *J. Chem.*  
658 *Phys.* 139 (2013) 244308.
- [51] M. Weiss, M. W. P. Strandberg, The microwave spectra  
659 of the deuterio-ammonias, *Phys. Rev.* 83 (1951) 567.
- [52] M. Lichtenstein, J. Gallagher, V. Derr, Spectroscopic  
660 investigations of the deuterio-ammonias in the millime-  
661 ter region, *J. Mol. Spectrosc.* 12 (1) (1964) 87–97.
- [53] F. C. De Lucia, P. Helminger, Millimeter-and  
662 submillimeter-wave length spectrum of the partially  
663 deuterated ammonias; a study of inversion, centrifugal  
664 distortion, and rotation-inversion interactions, *J. Mol.*  
665 *Spectrosc.* 54 (1975) 200–214.
- [54] E. Cohen, H. Pickett, The rotation-inversion spectra  
666 and vibration-rotation interaction in  $\text{NH}_2\text{D}$ , *J. Mol.*  
667 *Spectrosc.* 93 (1982) 83–100.
- [55] L. Fusina, G. Di Lonardo, J. Johns, L. Halonen, Far-  
668 infrared spectra and spectroscopic parameters of  $\text{NH}_2\text{D}$   
669 and  $\text{ND}_2\text{H}$  in the ground state, *J. Mol. Spectrosc.* 127  
670 (1988) 240–254.
- [56] H. M. Pickett, The fitting and prediction of vibration-  
671 rotation spectra with spin interactions, *J. Mol. Spec-*  
672 *trosc.* 148 (1991) 371–377.
- [57] M. Tafalla, P. Myers, P. Caselli, C. Walmsley,  
673 C. Comito, Systematic molecular differentiation in star-  
674 less cores, *Astrophys. J.* 569 (2) (2002) 815.
- [58] E. Keto, P. Caselli, Dynamics and depletion in ther-  
675 mally supercritical starless cores, *Mon. Not. R. Astron.*  
676 *Soc.* 402 (3) (2010) 1625–1634.
- [59] E. Redaelli, L. Bizzocchi, P. Caselli, O. Sipilä, V. Lat-  
677 tanzi, B. Giuliano, S. Spezzano, High-sensitivity maps  
678 of molecular ions in l1544-i. deuteration of  $\text{n}_2\text{h}^+$  and  
679  $\text{hco}^+$  and primary evidence of  $\text{n}_2\text{d}^+$  depletion, *Astron.*  
680 *Astrophys.* 629 (2019) A15.
- [60] S. Spezzano, S. Brünken, P. Schilke, P. Caselli,  
681 K. Menten, M. McCarthy, et al., Interstellar detection  
682 of  $\text{c-C}_3\text{D}_2$ , *Astrophys. J. Lett.* 769 (2) (2013) L19.
- [61] S. Spezzano, H. Gupta, S. Brünken, C. Gottlieb,  
683 P. Caselli, K. Menten, et al., A study of the  $\text{C}_3\text{H}_2$  iso-  
684 mers and isotopologues: first interstellar detection of  
685 HDCCC, *Astron. Astrophys.* 586 (2016) A110.
- [62] L. Bizzocchi, P. Caselli, S. Spezzano, E. Leonardo,  
686 Deuterated methanol in the pre-stellar core L1544, *As-*  
687 *tron. Astrophys.* 569 (2014) A27.